Acta Astronautica 229 (2025) 1–12

Contents lists available at ScienceDirect

Acta Astronautica

journal homepage: www.elsevier.com/locate/actaastro

Research paper

Rover ramp deployment system for Chandrayaan-3: Concept, design, development and operations

Akash A. Shetty, Harshit Kumar, Ramprasad Regulavalasa, Amit Kamboj, K. Prakasha, Raghavendra Prasad H.M., Gaurav Sharma *, Arun Kumar Gupta, Abhishek Kumar, Shankara A.

Spacecraft Mechanisms Group, U R Rao Satellite Centre, Indian Space Research Organisation, Old Airport Road, Vimanapura Post, Bengaluru, 560017, Karnataka, India

ARTICLE INFO

Keywords:
Chandrayaan-3
Lunar exploration
Lander
Rover
Ramp deployment system
Indian Space Research Organisation (ISRO)

ABSTRACT

Chandrayaan-3 is India's third lunar mission and its first successful landing on the Moon. It comprised a propulsion module, lander module and a rover housed within the lander module. To facilitate the rover's exit from the lander, a system with two separate deployable panels was used. These panels, driven by motors at the hinge lines, rigidify upon deployment to form a stable ramp. In the launch configuration, the rover was held on the primary panel using three hold-downs, while the panels were secured against the lander deck using another four hold-downs. Post lander touch-down, the panel hold-downs were released and the panels deployed to form a stable ramp. Subsequently, the rover hold-downs were released, allowing the rover to roll-out. The development process involved two models: Qualification model and Flight model. Qualification tests for ramp deployment and rover release were conducted using qualification hardware, confirming the design concept and its function, followed by acceptance level tests on the flight hardware. Chandrayaan-3 lander successfully landed near the Moon's south pole on August 23rd, 2023 and the ramp deployment facilitated the subsequent rover roll-out. This paper presents a comprehensive account of the concept, design, testing and post landing performance of Chandrayaan-3's rover ramp deployment system.

1. Introduction

The Indian Space Research Organisation (ISRO) has embarked upon a series of lunar exploration missions to further our understanding about its origin and evolution [1,2]. Chandrayaan-3 mission, launched on July 14th, 2023, featured Propulsion Module (PM), a Lander Module (LM), and a rover, with objectives encompassing a safe and soft landing near the moon's south pole, rover exploration, and the execution of in-situ scientific experiments. The PM and LM were mechanically integrated using an inter-module adapter, and the rover was accommodated within the LM (Figs. 1 and 2). Following the successful touchdown near the lunar southern pole on August 23rd, 2023, the rover ramp was deployed, facilitating the rover's roll-out onto the lunar surface.

The successful deployment of a rover onto extraterrestrial surface is a critical aspect of exploration missions beyond Earth. Over the last 53 years, fourteen rovers have been successfully deployed on the Moon, and Mars. These include crewed vehicles as well as remotely piloted and autonomous robots. Notable examples include United States' three crewed Lunar Roving Vehicle (LRV) [4] on-board Apollo 15, 16, and 17 missions, the Soviet Union's two Lunokhod lunar rovers [5,6], and China's two Chang'e rovers [7,8], which have explored the Moon. Similarly, the Soviet Union's Mars Prop-M rover [9], the United States' five rovers (Sojourner [10], Spirit [11], Opportunity [12], Curiosity [13], Perseverance [14]), and China's Tianwen-1 [15] rover have explored Mars.

In NASA's Apollo crewed missions, the astronauts manually deployed the LRV, which was stored in a folded state within one quadrant of the Lunar Module (LM) in a triangular envelope. The LRV's size was reduced to half its original length and 70 percent of its original width for storage and was secured by three structural hard points. Following a specific sequence, two astronauts unfurled the tightly packed LRV on the lunar surface and prepared its seats and other components [16].

There are two main options for rover deployment systems: frame type and arm-based system. Frame type ramp with side walls is the

* Corresponding author.
E-mail addresses: akashsh@ursc.gov.in (A.A. Shetty), harshitk@ursc.gov.in (H. Kumar), prasadrr@ursc.gov.in (R. Regulavalasa), amitkam@ursc.gov.in (A. Kamboj), kpra@ursc.gov.in (K. Prakasha), hmrp@ursc.gov.in (Raghavendra Prasad H.M.), gsrs@ursc.gov.in (G. Sharma), arun@ursc.gov.in (A.K. Gupta), abhishek@ursc.gov.in (A. Kumar), ashan@ursc.gov.in (Shankara A.).

https://doi.org/10.1016/j.actaastro.2024.12.014
Received 30 August 2024; Received in revised form 15 November 2024; Accepted 7 December 2024
Available online 21 December 2024
0094-5765/© 2024 IAA. Published by Elsevier Ltd. All rights are reserved, including those for text and data mining, AI training, and similar technologies.

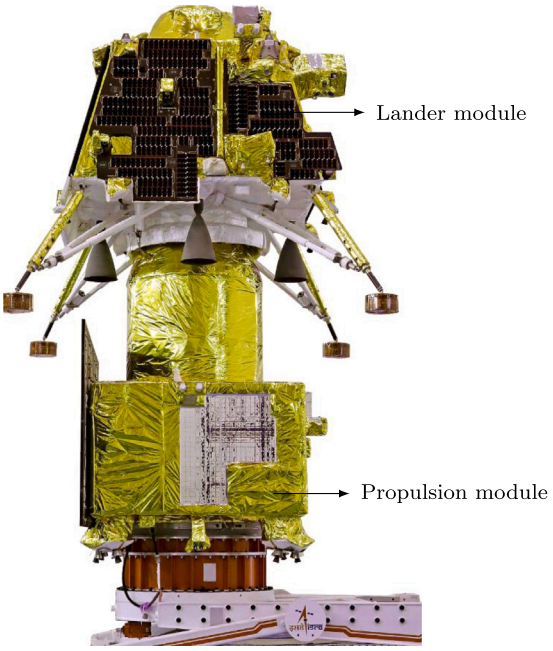

Fig. 1. Chandrayaan-3 CM on fixture [3].

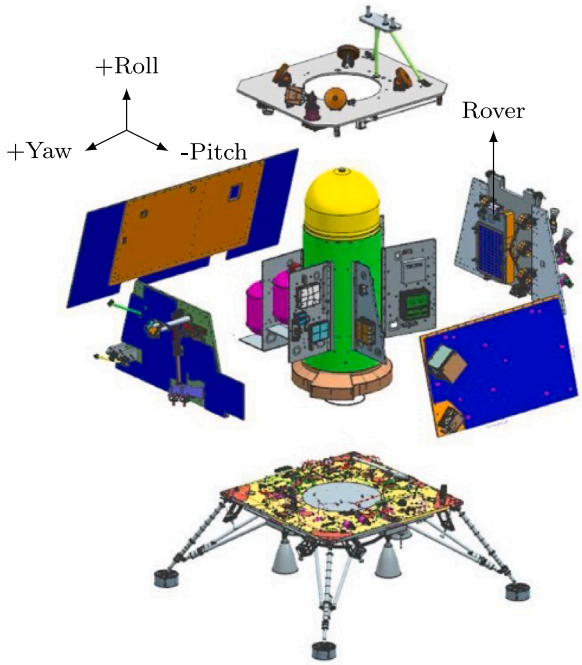

Fig. 2. Exploded view of LM.

most widely used rover deployment method, primarily due to its simplicity and reliability. It employs two individual ramp frames that extends from the lander onto the surface, allowing the rover to descend onto the ground.

Russia's Lunokhod 1 and Lunokhod 2 were deployed onto the lunar surface using the concept of dual-ramp roll-off [17]. The system utilized a pair of metallic frame type ramps to allow the rover to descend from the lander onto the lunar surface. The ramps were deployed from the lander in two directions, and the rover then carefully maneuvered down one of the ramps to the surface. The system has proven to be effective and reliable as it allowed both Lunokhods to successfully deploy to the lunar surface.

In Chang'e-3 mission, the rover was mounted on the top deck of the lander. Post landing on the Moon, the lander-rover connection was severed. Two frame type ramps, initially stored vertically on the lander's side panel, were horizontally deployed to allow the rover to transition from the top deck. An electro-mechanical system slowly lowered the ramp to the surface, ensuring a safe roll-off for surface exploration [18, 19]. A similar approach was employed to deploy Tianwen-1 Mars rover.

Arm-based systems offer greater flexibility and precision in rover deployment compared to ramp-based systems [20]. These systems utilize an articulated arm that extends from the lander, capable of maneuvering the rover to specific locations or orientations on the lunar surface. Arm-based systems are particularly advantageous for deploying rovers onto uneven terrain. NASA's InSight mars lander uses a robotic arm for moving instruments from the deck onto the ground [21]. The robotic arm, 1.8 m long, consisted of a grapple for grasping the hardware to be placed.

In all the above cases, the rover was mounted horizontally on top of the lander structure and frame-type ramps were used to aid the rover roll out. However, in the Chandrayaan-3 mission, placing the rover on top of the lander was not feasible, as the top deck of Chandrayaan-3's LM was already populated with scientific instruments. In contrast to previous rover missions, Chandrayaan-3's rover was positioned vertically within one of the LM's quadrants, as depicted in Fig. 2. It was done to utilize the empty space between deck and Spacecraft cylinder which led to the present configuration. Design was further simplified by mounting the rover to the ramp itself, thus eliminating the requirement for additional structural support.

Table 1
Parameters of rover.

Parameter	Value
Overall dimensions	750 mm (W) 917 mm (L) 397 mm (H)
Mass	26.5 kg

The deployment mechanism in Chandrayaan-3 thus had to serve a dual role: to support the rover throughout the spacecraft's mission phases and to facilitate deployment through a suitable mechanism when needed,unlike deployment mechanisms used in previous lunar missions.

Hence, a honeycomb panel-based system was configured, aligning with the unique demands posed by the rover's vertical placement inside the LM that also offered the advantage of shielding the rover from direct exposure to extreme thermal cycles, an environmental consideration in lunar missions.

The overall dimensions and the mass of the rover are shown in Table 1. Here, W is the maximum width of the rover along Pitch axis, L is the maximum length along Roll axis and H is the maximum height of the rover along Yaw axis with all of rover appendages in stowed condition.

This paper discusses the design and development of a Rover Ramp Deployment System (RRDS) for ISRO's Chandrayaan-3 mission. Section 2 highlights the design methodology of a ramp for a lunar landing mission and brings out the unique rover accommodation method employed, given the constraints imposed by the lander's primary structure. Sections 3–8 summarize the design and development of the ramp type RRDS including the tests. Section 9 discusses the telemetry data observed from launch till landing. Section 10 summarizes the post landing operations of the RRDS. Finally, Section 11 concludes the paper.

2. Design methodology

To accommodate the rover within the spacecraft's volume while withstanding the launch loads, it is imperative to implement a suitable mechanism that securely holds the rover during the spacecraft's journey

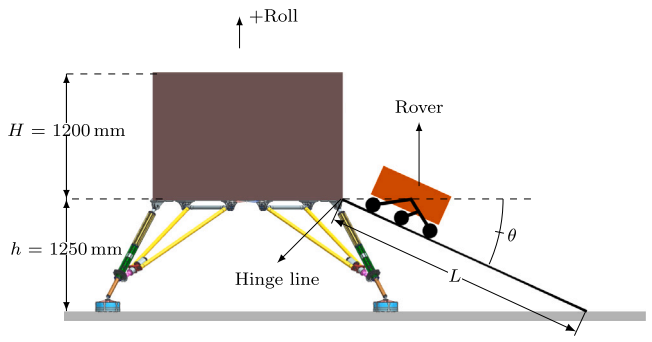

Fig. 3. Configuration of rover ramp.

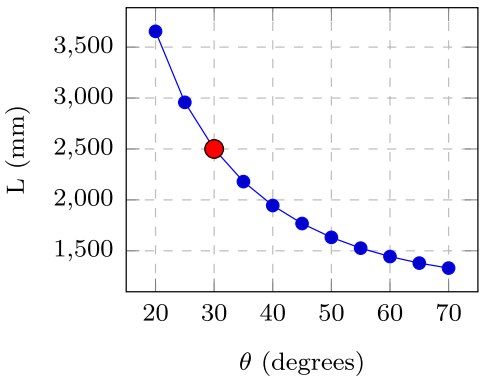

Fig. 4. Variation of the length L with the angle θ.

and facilitates its smooth deployment onto the lunar surface post-landing. Hence, the functional requirements encompass two primary aspects:

2.1. Functional requirement

1. Hold the rover securely, withstanding the dynamic forces during launch, transit to lunar orbit and the lunar descent.
2. Facilitate the controlled roll-out of the rover onto the lunar terrain with slope upto ±15°.

2.2. Concept

Fig. 3 shows the nominal landing scenario wherein the LM rests on the flat terrain with the ramp in deployed condition. The height of the deployed ramp's hinge line from the lunar surface (along the +Roll axis) measures 1250 mm in nominal condition. The rover schematic is not to scale in all figures that follow.

The length of the ramp (L) is worked out to ensure stability of the rover upon its hold-down release till roll down. Maximum size of ramp along roll axis in stowed configuration is constrained to a maximum of 1500 mm due to launch vehicle envelope. In a single-panel deployment system with $L \leq 1500$ mm the angle θ will be greater than 50° even for nominal terrain condition (Fig. 4). The rover mounted on the ramp is configured with a rocker-bogie based suspension mechanism with a static stability angle of 50°. The angle θ should be less than 35° to ensure rover stability for a terrain slope of 15° at landing site. Thus, $\theta = 30°$ is an adequate choice which demands a total ramp length of 2500 mm.

The friction between wheels and ramp is not sufficient to prevent rover from sliding at 30° angle. A rover wheel restraint mechanism is incorporated in the rover mobility system that prevents the rover from sliding during roll-down. The details are discussed in Section 5.

To accommodate a length of 2500 mm, it is proposed to implement a 2-panel foldable ramp. This design allows the folded ramp to be easily stowed within the lander structure, as illustrated in Fig. 5. The primary panel serves as the platform for mounting the rover and is connected to the LM's bottom deck through a primary hinge line. Similarly, the secondary panel is hinged to the primary panel via a secondary hinge line.

This option optimizes the use of space and ensures efficient stowage of the ramp. Furthermore, the utilization of a 2-panel foldable ramp allows for a seamless transition from stowed configuration to deployment, offering the necessary support for rover operations. The primary panel's pivotal attachment to the lander's bottom deck ensures stability during rover roll-down.

Two options were considered for deploying the panels to form a rigid ramp. In the first option, the secondary panel is deployed first, rotated by 180° using a motor along the secondary hinge line, and

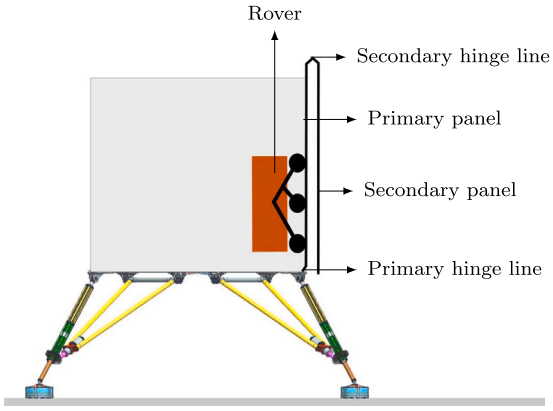

Fig. 5. Stowed configuration of the rover ramp.

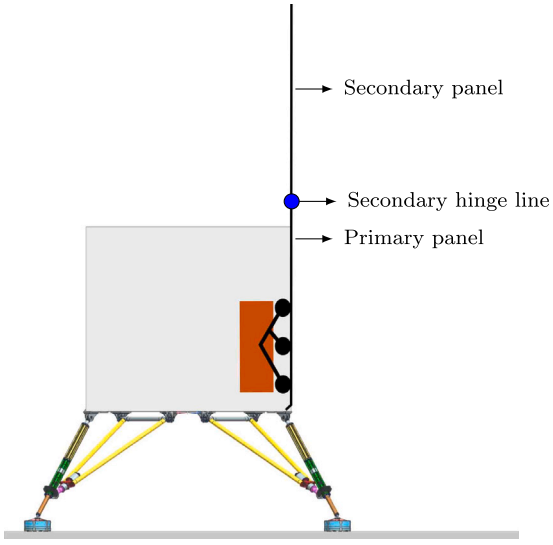

Fig. 6. Rover ramp with secondary panel deployed.

secured with the hinge latch (Fig. 6). Subsequently, the primary panel is deployed along with the already deployed secondary panel, reaching a nominal deployment angle of 120° from the vertical stowed position i.e. $\theta = 30°$

In the second option, a slider joint is placed between the primary and secondary panels. The primary panel is deployed using a motor along the primary hinge line, while the deployment of the secondary panel is gravity-assisted (Fig. 7).

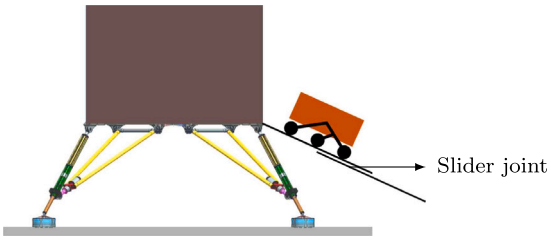

Fig. 7. Rover ramp with sliding secondary panel.

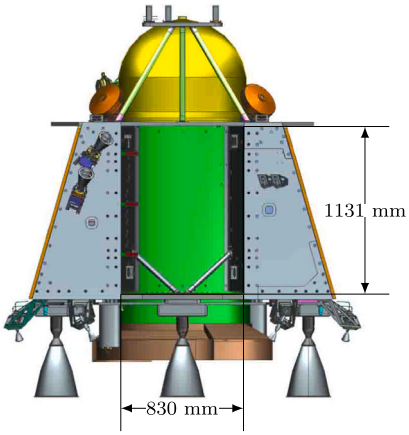

Fig. 8. Accommodation of ramp in -Yaw deck of LM.

Option 2 relies on sliding friction and gravity, both of which are uncertain depending upon the terrain slope and local features where ramp would touch on to the terrain. This uncertainty if catered to would lead to inclusion of an actuator in the arm, leading to design complexity. Option 1 on the other hand involves rotation of panels that does not get affected by the local terrain slope if the selected motor is able to withstand the gravity torque induced about the rotation axis. Based on relative advantages of option-1 over option-2, it has been considered for the present case.

3. Hold-down and release mechanism

From launch until touchdown on the lunar surface, both the primary and secondary panels should be held in stowed position to withstand the launch and landing loads. Post landing, both the panels should be released with minimal shock, allowing them to unfold and function as intended. Hence a non-explosive Frangibolt actuator [22] based Hold-Down Release Mechanism (HDRM) is configured. The actuator is based on Shape Memory Alloy (SMA), which expands upon heating and cuts the bolt at the notched section, facilitating the separation of primary and secondary panels from the structure. The hold-down is configured such that the bolt's notch section aligns with the separation plane.

3.1. Sizing of rover ramp panels

To accommodate the rover inside the lander and to subsequently deploy it onto the lunar surface, a cutout with specific dimensions is included on the -Yaw axis deck of the LM (Fig. 8). The rover's maximum dimension along the Pitch axis is 750 mm, and the cutout on the LM -Yaw deck has a maximum width of 830 mm, ensuring sufficient clearance. Finalized primary and secondary panel dimensions, as shown in Table 2, account for the need to accommodate hold-down interfaces for securely stowing the panels.

Both panels are integrated with Carbon Fiber Reinforced Polymer (CFRP) guide paths to guide the rover along the ramp during rover hold-down release and subsequent roll-out.

Table 2
Parameters of primary and secondary panel.

Parameter	Primary panel	Secondary panel
Width	870 mm	930 mm
Length	1130 mm	1310 mm
Thickness	40 mm	15 mm
Material	AA-6061 honeycomb with CFRP face sheet	
Mass	4.4 kg	1.5 kg

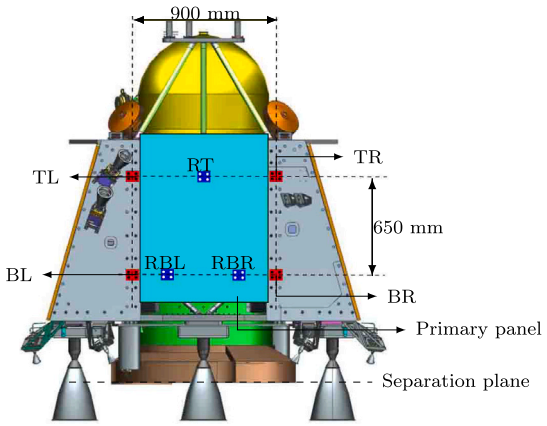

Fig. 9. Configuration of HDRM.

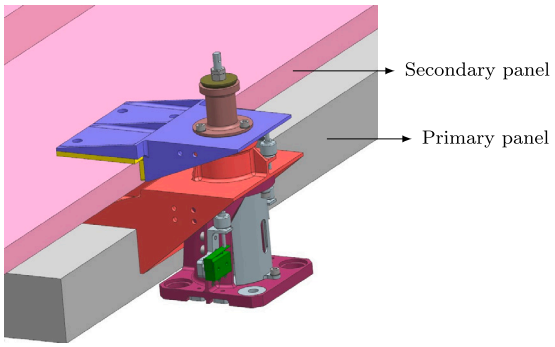

Fig. 10. Bottom hold-down assembly with panels.

3.2. Hold-down locations

The rover is held to the primary panel at three locations: one at the top (RT) and two at the bottom side of the rover (RBL and RBR). The rover ramp HDRM is configured with four hold-down points, two at the top (TL - Top Left and TR - Top Right) and two at the bottom (BL–Bottom Left and BR–Bottom Right). The locations of the rover ramp hold-downs along the Roll axis are such that they align with the rover hold-downs; TL and TR align with RT, and BL and BR align with RBL and RBR (Fig. 9). This alignment ensures that the four ramp hold-downs take the maximum share of the inertial load due to rover (Tables 3–5).

3.3. Hold-down configuration

The lower hold-down assembly securely holds both the primary and secondary panels using their respective brackets, as depicted in Fig. 10. On the other hand, the upper hold-down assembly exclusively secures the primary panel to the lander deck.

3.4. Hold-down system

Each of the HDRM comprises a hold-down base, affixed to the negative Yaw panel of the lander craft, featuring a circular spigot on its

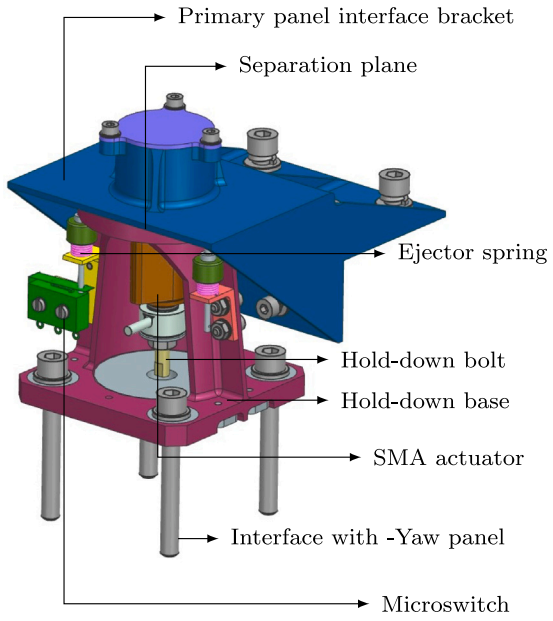

Fig. 11. Top hold-down assembly.

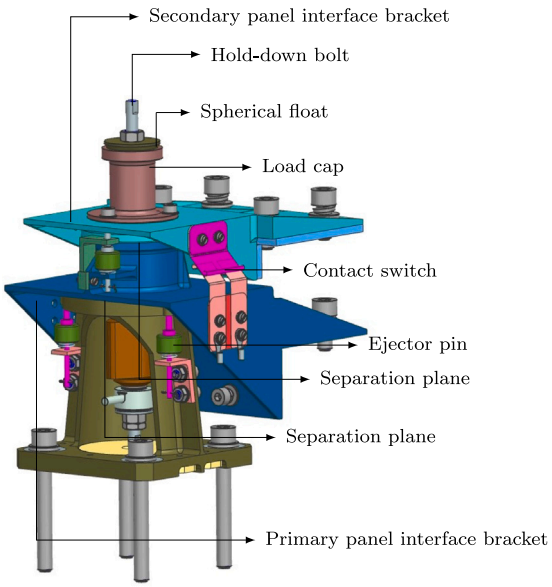

Fig. 12. Bottom hold-down assembly.

top surface. The Frangi actuator is housed inside the hold-down base. The corresponding mating component, the primary panel/secondary panel interface bracket, is mounted on the ramp panel, serving as the mating part for the spigot (Figs. 11 and 12).

The Frangi actuator consists of a heater attached to a shape memory alloy cylinder, enclosed by a thermal insulating jacket. A Titanium alloy bolt with a notch, connects the fixed and moving elements. When powered on, the actuator regains its shape, creating tension in the bolt and compression in the joint. If the joint has low thermal conductivity, the actuator can expand enough to break the bolt at the notch, separating the structures without jamming. Anodized Titanium washers limit heat transfer between the actuator and the structure. Proper heat balance is crucial for the actuator to elongate and apply the necessary tensile load to cause bolt failure [23]. Successful implementation requires a housing, a stiff joint design, and an appropriate thermal path (Fig. 13).

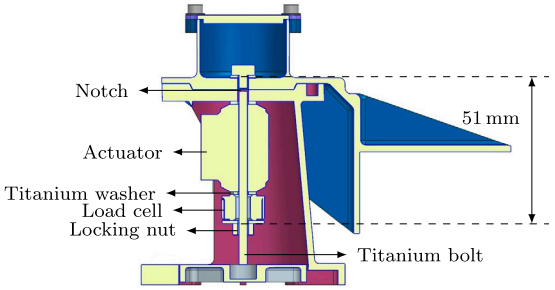

Fig. 13. Section view of top hold-down.

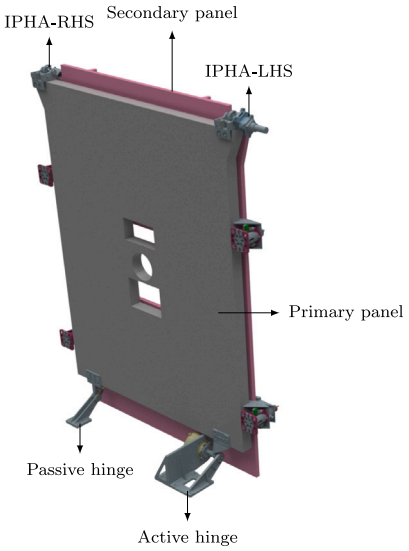

Fig. 14. Drive mechanism.

A load cell is incorporated to measure the amount of the preload in the hold-down bolt. The hold down assembly storage temperature should be maintained between −65 °C to 85 °C to avoid self-actuation.

In line with the deployment sequence, the two bottom hold-downs are released, followed by controlled deployment of the secondary panel. Subsequently, the top two hold-downs are actuated, facilitating the release of the primary panel. Each hold-down assembly comprises a status indication for the release. A pair of ejector springs, ensure initial separation after the hold-down bolt is cut.

4. Drive mechanism

Two hinge line drive mechanisms are configured to deploy the secondary and primary panels post hold-down release (Fig. 14).

4.1. Secondary hinge line drive mechanism

The connection between the primary and secondary panels involves a set of Inter-Panel Hinge Assembly (IPHA), with one hinge incorporating a stepper motor. This motor facilitates the deployment of the secondary panel to a 180° angle. On the non-motor side hinge, there is a potentiometer to monitor the deployment angle, and the motor side hinge is equipped with a micro-switch to confirm the deployment of the secondary panel.

The total moving mass of the secondary panel (m_{sec}) is 3.6 kg with its CG (CG_{sec}) at a distance of 0.672 m from the secondary hinge line. The torque required to drive the panel is maximum when the secondary

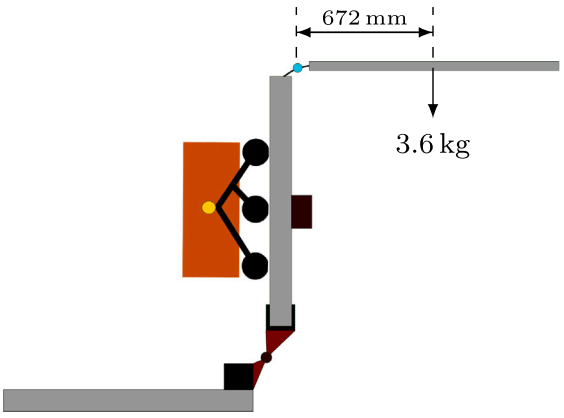

Fig. 15. Secondary panel deployed by 90°.

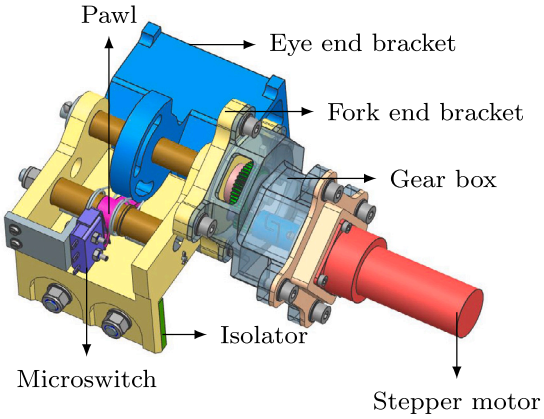

Fig. 16. IPHA-LHS in stowed configuration.

panel is deployed by 90° ($T_{sec_{max}}$) is given as (Fig. 15)

$$T_{sec_{max}} = m_{sec} \times CG_{sec} \times \frac{g_{earth}}{6} \tag{1}$$

In the above equation, g_{earth} is the acceleration due to gravity on the Earth. From Eq. (1), the maximum torque required to drive the secondary panel is 3.95 N m. The gravity constant on moon is nearly one sixth of that on the earth and the same has been used for torque calculations.

4.1.1. Inter-panel hinge assembly-LHS

The LHS hinge features a motorized mechanism incorporating a simple gear train. This hinge assembly comprises a fork-end mounted on the primary panel with a stepper motor mounting interface, while the eye-end bracket interfaces with the secondary panel. The fork-end incorporates a locking mechanism consisting of a pawl and pawl shaft mechanism, ensuring secure hinge locking at the end of deployment. A micro-switch mounted on the fork end bracket confirms the latch status upon deployment (Fig. 16).

The secondary gear box incorporates a simple gear train with a gear ratio of 1:2. The maximum torque provided by driveline at output shaft of secondary gear box (T_G) is given by

$$T_G = T_M \times 2 \times \eta_G \tag{2}$$

In the above equation, $\eta_G = 0.97$, is the gear efficiency of secondary gear box and T_M is the torque capacity of motor gear head. From Eq. (2), a torque T_G of 9.7 N m establishes a margin of greater than 1 over the required torque $T_{sec_{max}}$.

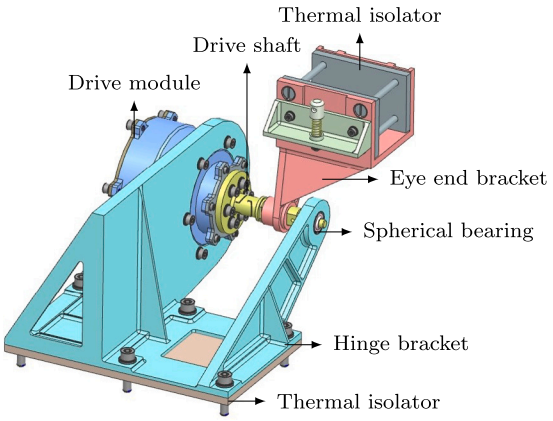

Fig. 17. Active hinge assembly in stowed configuration.

4.1.2. Inter-panel hinge assembly-RHS

The RHS hinge fork and eye ends share a design similar to the LHS hinge. Nevertheless, the RHS hinge is passive. Instead, it incorporates a potentiometer to monitor the deployment angle of the secondary panel.

4.2. Primary hinge line drive mechanism

The primary hinge line consists of an Active Hinge (Fig. 17) and a Passive Hinge mounted on either side of the primary panel. The drive torque is provided by a stepper motor-based drive module on the active hinge side. A potentiometer, located on the passive hinge, provides information on the deployment angle of the panel. The nominal deployment angle is 120°, and the hinge mechanism can provide up to 130° if required, depending on the lander landing terrain conditions. To allow for this freedom of varied deployment angles, no latch mechanism is provided between the rover panel and lander. The total moving mass is 45.5 kg.

4.2.1. Drive module

The deployment of the rover unfolds in two distinct phases, each serving a crucial role in the controlled descent of the rover and panel stack assembly on the lunar surface (Fig. 18).

Phase 1. In this initial stage, motor has to drive the rover and panel stack assembly against lunar gravity as it lifts the overall CG, requiring a positive deployment torque. This phase lasts till the CG reaches the maximum height (Fig. 19).

Phase 2. As the rover and panel assembly deploys by more than 14.5°, a critical shift occurs and the CG height begins to reduce (Figs. 19 and 20). This phase demands precise control to ensure a regulated and safe descent. Within Phase-2, the drive mechanism takes on the role of providing a controlling torque. This torque is instrumental in governing the deployment of the rover, preventing uncontrolled rotation of the panel.

Eq. (3) and Fig. 20 show the variation in the required torque at the primary hinge line (T_{pri}) as the ramp deploys from its initial stowed position. The drive module design considers the torque requirements for both phases. The emphasis is to ensure adequate margin over the maximum torque needed to facilitate a controlled deployment on the lunar surface.

$$T_{pri} = \left[\left(m_{sec} \times CG_{sec} + m_{pri} \times CG_{pri}\right) \times \sin\phi + m_{rover} \times CG_{rover} \times \sin(\phi - 14.5°)\right] \times \frac{g_{earth}}{6} \tag{3}$$

In the above equation, m_{pri}, m_{rover}, CG_{pri}, and CG_{rover} are the masses and CGs from the primary hinge line of primary panel, and

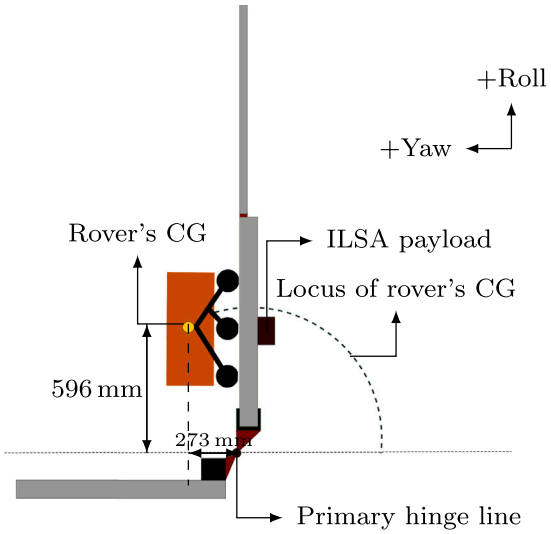

Fig. 18. Beginning of Phase-1 deployment.

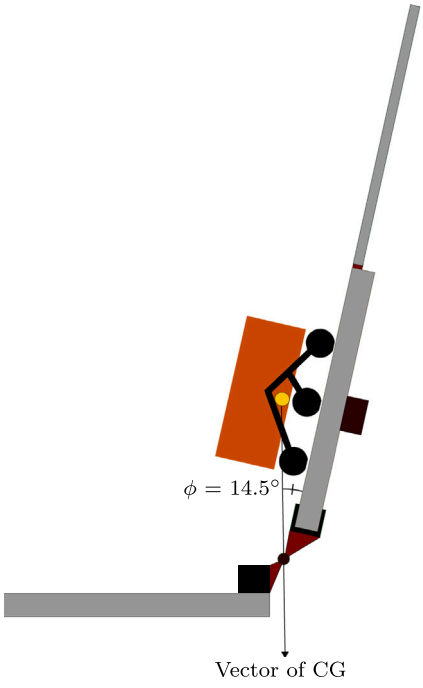

Fig. 19. Unstable equilibrium position.

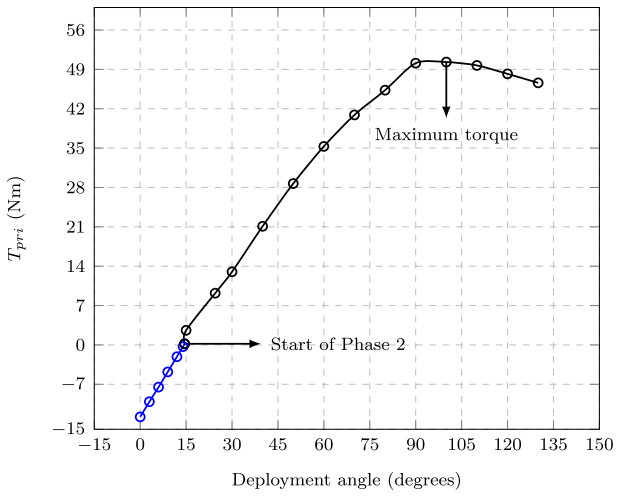

Fig. 20. Required drive torque vs. deployment angle.

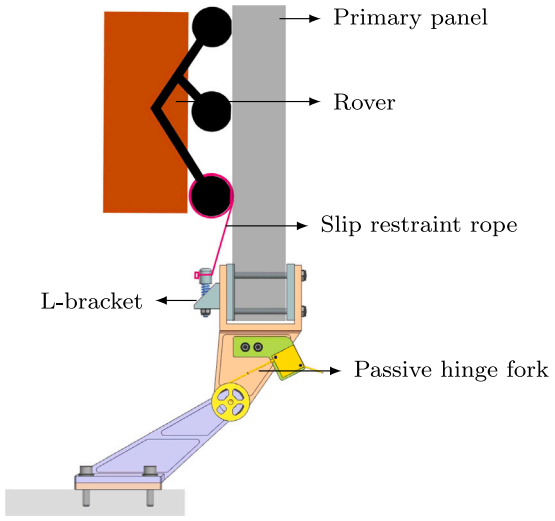

Fig. 21. Configuration of slip restraint mechanism (Rover schematic not to scale).

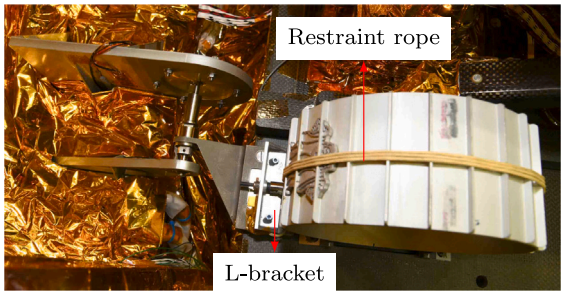

Fig. 22. Implementation of slip restraint mechanism in Chandrayaan-3.

rover respectively. The maximum torque of 50 Nm required at 100° deployment angle is within the powered holding torque capacity of 75 Nm.

The drive module is a stepper motor based compact actuator designed around harmonic drive. Grease lubricated and pre-loaded duplex bearings are used to withstand launch, lading and deployment loads.

5. Slip restraints

The controlled roll out of the rover over the ramp is ensured by the rover restraint mechanism. The restraints utilizes a Kevlar rope to control the rover's sliding on the ramp. One end of the Kevlar rope contains a planar Be-Cu flat spring and supporting pins, which are pressed against a grouser on rear wheels. The rope is wound around the wheels along the grooves provided on the grousers. The flat spring helps in releasing the rope from the wheel's grouser at the end of unwinding. The other end of the rope is held by an L-bracket mounted on the eye end of the active and passive hinge assemblies, as shown in Figs. 21 and 22. A compression spring in the bracket provides the necessary tension in the rope.

During the rover's roll-out from the ramp, the Kevlar rope wound over the rover's rear wheels will start unwinding. Before the wheel touches the lunar surface, the rope's tip slips out of the groove. The length of the wound rope is around 2 m, ensuring that the rear wheel

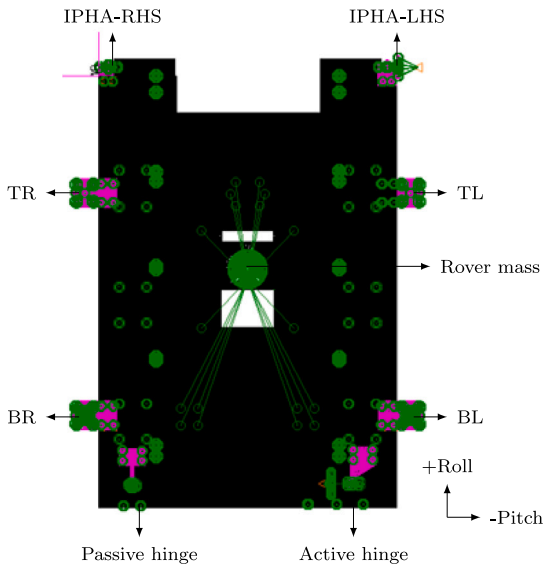

Fig. 23. FE model of rover ramp (view along Yaw axis).

Table 3
Forces along Yaw axis for inertial load along Yaw axis.

Location	Force (N)	Load shared, %
TL	3527	30.6
TR	3370	29.2
BL	1937	16.8
BR	2001	17.4
Active hinge	431	3.7
Passive hinge	256	2.2
Total	**11,522**	**100**

is released from the rope just before touching the lunar surface. This ensures a smooth, slip-free movement of the rover on to the lunar terrain.

6. Finite element analysis

The integrity of the ramp in held condition was ascertained through Finite Element (FE) analysis that provided pre-load requirement for the hold down and adequacy of bearing strength to withstand the launch loads. FE model of the rover ramp deployment mechanism assembly is developed by integrating the mathematical model of primary and secondary panels with the mechanism components (Figs. 23 and 24).

Quasi-Static Load (QSL) of 25 g inertial acceleration is considered independently along all three directions. The resultant loads acting on hinges and hold-downs are detailed in Tables 3, 4, and 5. From Table 3, it is evident that hold-downs withstand approximately 92% of the total load. The peak pull-out load at the hold-down is 3527 N. Consequently, a preload of 5400 N is provided for the hold-down bolt (along Yaw axis). The normal modes are estimated for the RRDS with rigid boundary conditions. The dominant primary and secondary modes were estimated to be 61 Hz and 73 Hz respectively. In Table 4, force along passive hinge is zero due to provision of hinge float along Pitch direction.

7. Ground gravity compensation system

The ground deployment tests involve utilizing Helium filled balloons to assist in deploying primary and secondary panels, simulating loads during lunar gravity conditions. The approach accurately replicates the motor's moment requirements for driving the rover ramp throughout the deployment on the moon. The test system consists of

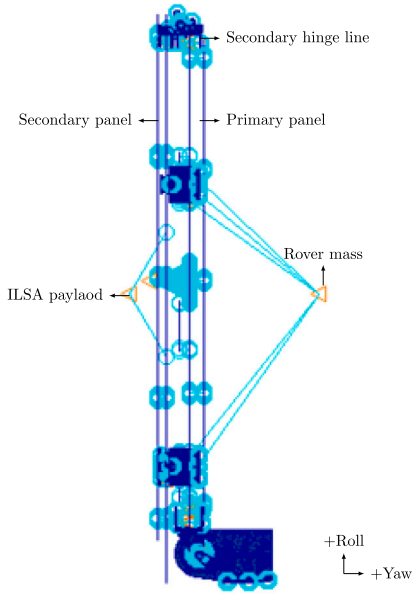

Fig. 24. FE model of rover ramp (view along Pitch axis).

Table 4
Forces along pitch axis for inertial load along pitch axis.

Location	Force (N)	Load shared, %
TL	2924	25.4
TR	2890	25.1
BL	2300	20.0
BR	2380	20.7
Active hinge	1026	8.9
Passive hinge	0	0
Total	**11,520**	**100**

Table 5
Forces along roll axis for inertial load along roll axis.

Location	Force (N)	Load shared, %
TL	1550	13.5
TR	1740	15.1
BL	2324	20.2
BR	2571	22.3
Active hinge	2360	20.5
Passive hinge	972	8.4
Total	**11,517**	**100**

a balloon, a horizontal bar and a pair of slings that connects the panel to the horizontal bar (Fig. 25). The moment about the drive hinge line due to drag force is neglected because of the lower deployment rate (primary panel: $0.77\,^\circ\,s^{-1}$ and secondary panel: $0.93\,^\circ\,s^{-1}$). A spherical joint is provided at the panel-sling interface to keep the sling vertical throughout the deployment.

7.1. Deployment of secondary panel

Fig. 26 shows the schematic when secondary panel is deployed by 90°. Maximum moment about the secondary hinge line ($M_{sec_{max}}$) when the panel is at 90° while deploying on the Earth is

$$M_{sec_{max}} = m_{sec} \times CG_{sec} \times g_{earth} = 23.7\,\text{N m} \quad (4)$$

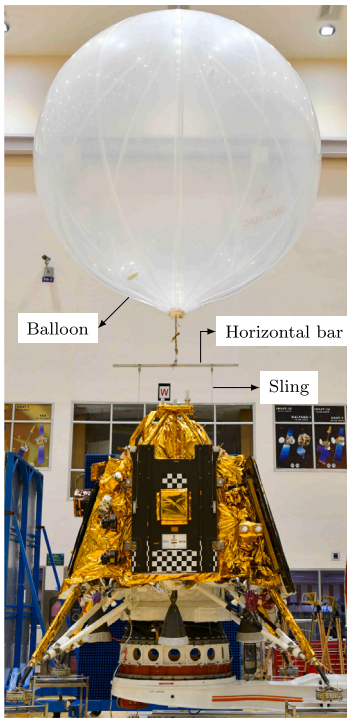

Fig. 25. Balloon assisted deployment of secondary panel.

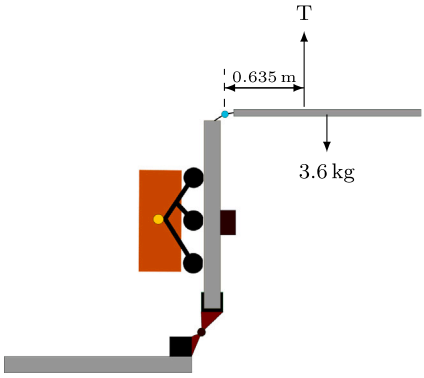

Fig. 26. Maximum balloon lift required in deploying secondary panel.

To simulate the lunar conditions on Earth, the compensating moment (M_{sec_c}) required is

$$M_{sec_c} = M_{sec_{max}} - T_{sec_{max}} = 19.8\,\text{N m} \tag{5}$$

The total lift ($T_{balloon_{pri}}$) required in the balloon (Fig. 26) is calculated as.

$$T_{balloon_{sec}} = \frac{M_{sec_c}}{CG_{sec}} = 31.2\,\text{N} \tag{6}$$

The balloon lift should also completely offload the mass of the fixtures (12.7 N) used to connect the balloon to the secondary panel. Hence, the total lift required in the balloon is 43.9 N

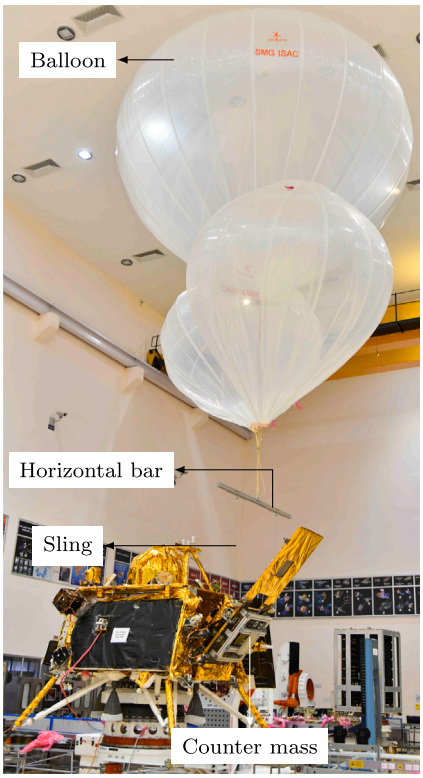

Fig. 27. Balloon assisted deployment of primary panel.

7.2. Deployment of primary panel

For the primary panel, the slings are connected to the center of the edge face. When deploying the primary panel, a counter mass (Fig. 27) is incorporated on the side opposite to the rover mounting face. This is done to replicate the drive torque requirement during Phase 1 (Fig. 20) while testing on ground.

The total moving mass of RRDS (m_{tot}) is 67.5 kg on ground (including counter-mass of 22 kg) with CG (CG_{tot}) at 0.678 m .

$$M_{pri_{max}} = m_{tot} \times CG_{tot} \times g_{earth} \tag{7}$$

From Eq. (4), we get $M_{pri_{max}} = 449\,\text{N m}$. To simulate the lunar conditions on Earth, the compensating moment (M_{pri_c}) required is

$$M_{pri_c} = \frac{5}{6} \times M_{pri_c} = 374.2\,\text{N m} \tag{8}$$

The balloon is connected at a distance of 1.107 m from the primary hinge line. The total lift ($T_{balloon_{pri}}$) required in the balloon is calculated as

$$T_{balloon_{pri}} = \frac{M_{pri_c}}{CG_{pri}} = 338\,\text{N} \tag{9}$$

The balloon lift should also offset the mass of the fixtures (66.2 N) used to connect the balloon to the primary panel. Hence, the total lift required is 404.2 N. The overall sequence of deployment is shown in Fig. 28.

8. Qualification tests

To test RRDS for environmental loads, drive level thermo vacuum test and system level vibration test was carried out. Tests were done to qualification level for thermovac and protoflight for vibration. Fig. 29 shows the qualification test campaign for the Qualification Model (QM)

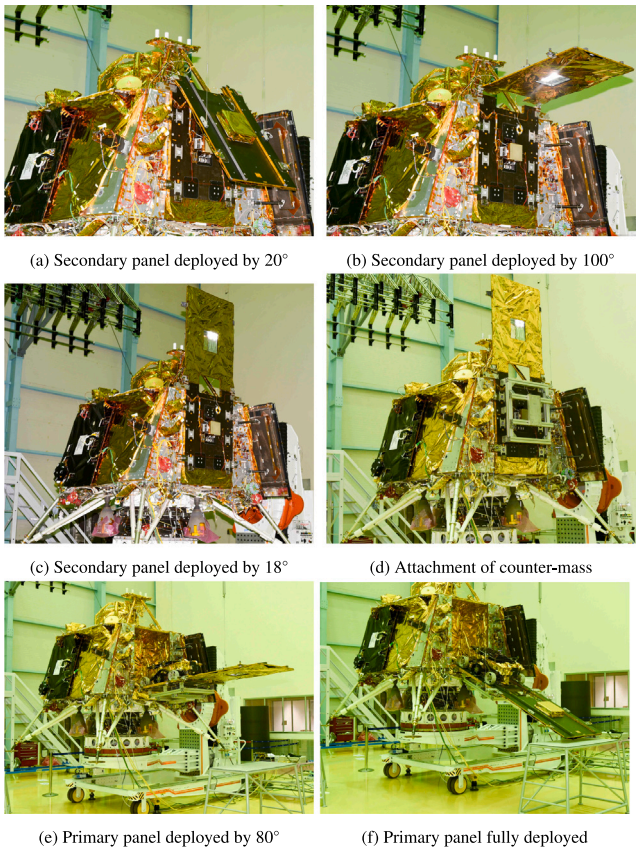

(a) Secondary panel deployed by 20° (b) Secondary panel deployed by 100°

(c) Secondary panel deployed by 18° (d) Attachment of counter-mass

(e) Primary panel deployed by 80° (f) Primary panel fully deployed

Fig. 28. Sequence of deployment.

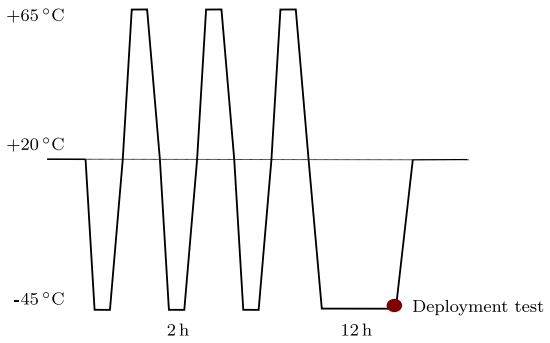

Fig. 29. TVT profile.

consisted of Thermal Vacuum Tests (TVTs) and Vibration Tests (VTs) conducted at both unit and assembly levels. Performance tests were executed before and after these tests to verify system functionality. To verify the performance of the primary and secondary drive mechanisms under extreme temperatures, a test setup was designed to simulate the moment load on the drive hinge lines, equivalent to the expected load during lunar deployment. After achieving a successful vacuum, the setup underwent three thermal cycles between −45 °C and 65 °C. Performance testing was conducted following a 12 h soak at −45 °C of the chamber's base plate Fig. 29. Before initiating motor operations, heaters mounted on the motor casing were activated to achieve the required operating temperature range (0 to 60 °C). Both drive mechanisms performed nominally without any degradation.

The QM model, with the stowed RRDS, was subjected to Proto-Flight Level Sine (PFLS) vibration tests. Low-Level Random (LLR) and Low-Level Sine (LLS) signature tests were performed both before and

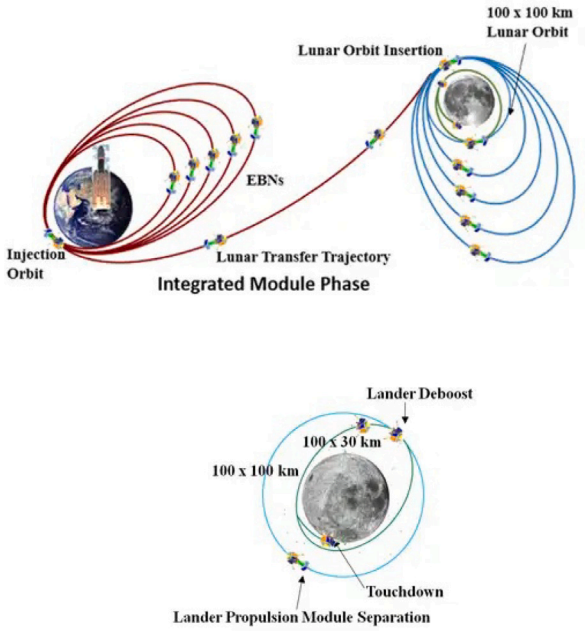

Fig. 30. Mission profile of Chandrayaan-3.

after the PFLS to monitor structural responses and health. LLR tests were conducted prior to LLS tests to establish a notching plan for LLS. An Intermediate Level Sine (XILS) test was conducted before the XPFLS along the X-axis to prevent overtesting due to system non-linearity. From the low-level sine signature tests, the primary and secondary panels' first modes were identified at 42.8 Hz and 60.8 Hz, respectively. These modes were well separated from the structure's and other subsystems' modes and observed to be lower than the subsystem level estimated value due to deck flexibility. Following dynamic testing, RRDS deployment tests were successfully executed with no mechanical anomalies. All four hold-downs functioned nominally. Post-VT, the QM model was subjected to a drop test from a height of 692 mm, achieving a vertical velocity of 2.5 ms^{-1}. The RRDS's integrity was confirmed through preload measurements at the hold-downs, with preload drops remaining below 5% pre- and post-test, indicating system integrity.

Based on the above results, a flight model assembly was developed following the same design concept. The flight model underwent acceptance level tests, including deployment tests, to validate system functionality.

9. Mission phases and telemetry insights

Following the Chandrayaan-3 launch, key mission phases included Earth Burns (EBN), Translunar Injection (TLI), Lunar Burns (LBN), PM-LM separation, Lunar Orbit Insertion (LOI), and two Deboost (DOB) operations before the final powered descent and touchdown (Fig. 30).

Throughout, telemetry data indicated nominal parameters for contact switches/micro-switch on the RRDS. Temperature changes in hold-downs and motors were monitored, with motor temperatures consistently maintained within the storage limit of −45 °C to 60 °C during maneuvers. Ramp hold-down temperatures, influenced by spacecraft's rotation, were kept within the storage limit of −80 °C to 65 °C by minimizing direct sun exposure to the -Yaw panel to prevent self-actuation of frangi actuators.

10. Post landing deployment and operations

The ramp mechanism was deployed after nearly 2 hours of landing so as to allow sufficient time for the regolith to settle down and also

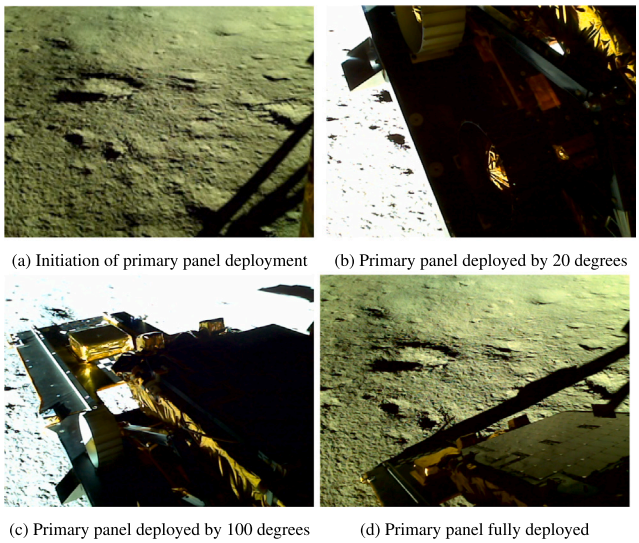

(a) Initiation of primary panel deployment (b) Primary panel deployed by 20 degrees

(c) Primary panel deployed by 100 degrees (d) Primary panel fully deployed

Fig. 31. Deployment of primary panel.

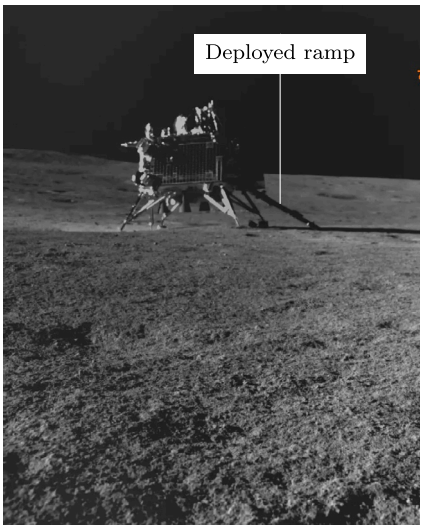

Fig. 32. Lander with deployed ramp.

to maintain the thermal requirements aspects of the various systems of the lander etc. The developed mechanism's functioning depends on the successful release of the hold downs and the actuation of deployment motors. The hold-downs and drive modules were covered to protect against lunar dust. The sequence of operation included actuation of hold-downs BL and BR, followed by rotation of secondary panel. Subsequently, TL and TR hold-downs were released followed by primary ramp deployment.

The temperatures of BL and BR actuators were −10 °C and 3 °C respectively, before heating. The actuators were heated till actuation, which was confirmed by the change in contact-switch status to *Released*. BL's contact switch briefly toggled to *Released* for 3.5 s. Motor dual coil excitation was *Enabled* and the secondary panel was rotated by 150 steps (2.25°) to confirm first motion. BL's release status changed to *Released* at rotation start which was followed by rotation by 11 850 steps (177.75°) for latching. The potentiometer indicated a net deployment of 175.3° which compared well with the on-ground reading of 176.6°. The difference is attributed to the coarse resolution and least count error of 0.97°. The latch status confirmed the successful deployment of secondary panel.

The temperature of TL actuator was −10 °C before actuation, which was confirmed by change in micro-switch status. Motor auto-hold was *Enabled* followed by heating of TR actuator which was at 11 °C at start of heating. The primary panel was rotated by 17 600 steps (110°). Frangi bolt actuation time for holddowns on lunar surface was observed to be around 35 s, which is slightly higher than the on-ground observed actuation time of 27–30 s at ambient temperature. The potentiometer angle changed from 2.7° to 103° in 168 s, settling at 122.2° when motor auto-hold was *Disabled*. The motor temperature rose from 20 °C to 30 °C over 9 min and 14 s during auto-hold *Enable*. Primary panel deployment is shown in Fig. 31. The deployed ramp as seen by the rover is in Fig. 32.

After the deployment of the rover ramp, the rover was successfully rolled out of the ramp. It carried out in-situ exploration of the lunar terrain for one lunar day. The rover motion on lunar surface resulted in few important discoveries. The exploration of the lunar terrain near South pole has led to further understanding of the elemental abundance measurements [24] and the landing site evolution [25].

11. Conclusion

This paper discussed the design, development, and implementation of a rover deployment system onboard Chandrayaan-3. The system utilized a foldable ramp mechanism comprising a primary and secondary panel to deploy the rover onto the lunar surface. The rover was affixed to the primary panel, connected to the lander module, while the secondary panel was hinged to the primary panel, both driven by motors along the hinge line. The deployment mechanism incorporated a frangi actuator-based HDRM.

FE analysis was conducted to analyze load distribution among hinges and hold-downs and calculate the required hold-down preload. Extensive qualification tests were performed on a qualification model at both unit and system levels, including deployment tests to ensure system's reliability. Vibration tests confirmed the HDRM and deployable system's resilience during launch, while a cold functional test in a thermo-vacuum chamber validated functionality in near-vacuum conditions. Based on the qualification model's results, a flight model assembly was developed following the same design concept. The flight model underwent acceptance level tests, including deployment tests, to validate system functionality. Following the Chandrayaan-3 lander's successful touchdown, the deployment mechanism operated effectively on the moon's surface.

The foldable ramp mechanism has proven to be a vital element in lunar surface exploration, as demonstrated by its successful deployment during the Chandrayaan-3 mission. The rigorous testing and validation processes undertaken validate the reliability and functionality of the deployment mechanism, affirming its suitability for future lunar and planetary missions.

CRediT authorship contribution statement

Akash A. Shetty: Writing – original draft, Validation, Methodology, Data curation. **Harshit Kumar:** Visualization, Data curation. **Ramprasad Regulavalasa:** Visualization. **Amit Kamboj:** Visualization, Formal analysis. **K. Prakasha:** Methodology. **Raghavendra Prasad H.M.:** Supervision, Methodology, Data curation. **Gaurav Sharma:** Writing – review & editing, Validation, Investigation, Formal analysis. **Arun Kumar Gupta:** Writing – review & editing, Validation, Supervision, Methodology, Investigation, Conceptualization. **Abhishek Kumar:** Writing – review & editing, Supervision. **Shankara A.:** Writing – review & editing, Supervision, Conceptualization.

Declaration of competing interest

The authors declare that they have no known competing financial interests or personal relationships that could have appeared to influence the work reported in this paper.

Acknowledgments

The RRDS was developed by the Spacecraft Mechanisms Group at URSC in Bengaluru, with panels from the Structures Group, thermal design by the Thermal Systems Group, and support from the Facilities Group. The authors thank the design review committee, senior colleagues, and the URSC Director for their consistent support.

References

[1] J.N. Goswami, M. Annadurai, Chandrayaan-1 mission to the Moon, Acta Astronaut. 63 (11–12) (2008) 1215–1220.
[2] S. Mathavaraj, K. Negi, G. Vaibhav, ISRO's unprecedented journey to the Moon, Acta Astronaut. 177 (2020) 286–298.
[3] Chandrayaan-3 Image Gallery, Indian Space Research Organisation, 2024, from https://www.isro.gov.in/chandrayaan3_gallery.html. (Retrieved 12 July 2024).
[4] Apollo Lunar Roving Vehicle (LRV), National Space Science Data Center, 2024, from https://nssdc.gsfc.nasa.gov/planetary/lunar/apollo-lrv.html. (Retrieved 16 February 2024).
[5] Spacecraft Display: 1970-095A, National Space Science Data Center, 2024, from https://nssdc.gsfc.nasa.gov/nmc/spacecraft/display.action?id=1970-095A. (Retrieved 16 February 2024).
[6] Spacecraft Display: 1973-001A, National Space Science Data Center, 2024, from https://nssdc.gsfc.nasa.gov/nmc/spacecraft/display.action?id=1973-001A. (Retrieved 16 February 2024).
[7] Spacecraft Display: 2013-070A, National Space Science Data Center, 2024, from https://nssdc.gsfc.nasa.gov/nmc/spacecraft/display.action?id=2013-070A. (Retrieved 16 February 2024).
[8] Spacecraft Display: 2018-103A, National Space Science Data Center, 2024, from https://nssdc.gsfc.nasa.gov/nmc/spacecraft/display.action?id=2018-103A. (Retrieved 16 February 2024).
[9] Spacecraft Display: 1971-049F, National Space Science Data Center, 2024, from https://nssdc.gsfc.nasa.gov/nmc/spacecraft/display.action?id=1971-049F. (Retrieved 16 February 2024).
[10] Mars Pathfinder Sojourner Rover, NASA, 2024, from https://rps.nasa.gov/missions/5/mars-pathfinder-sojourner-rover/. (Retrieved 16 February 2024).
[11] MER Spirit, NASA, 2024, from https://science.nasa.gov/mission/mer-spirit/. (Retrieved 16 February 2024).
[12] MER Opportunity, NASA, 2024, from https://science.nasa.gov/mission/mer-opportunity/. (Retrieved 16 February 2024).
[13] Mars Science Laboratory (MSL) - Curiosity Rover, NASA, 2024, from https://mars.nasa.gov/msl/home/. (Retrieved 16 February 2024).
[14] Mars 2020 Rover, NASA, 2024, from https://mars.nasa.gov/mars2020/. (Retrieved 16 February 2024).
[15] Spacecraft Display: 2020-049A, National Space Science Data Center, 2024, from https://nssdc.gsfc.nasa.gov/nmc/spacecraft/display.action?id=2020-049A. (Retrieved 16 February 2024).
[16] A.B. Hunter, B.W. Spacey, Lunar roving vehicle deployment mechanism, in: 7TH Aerospace Mechanisms Symposium, NASA Johnson Space Center, 1972.
[17] T. Balint, Summary of russian planetary lander mission, in: Deep Space Mission Architecture Group, Vol. 311B, NASA-JPL, 2002, pp. 1–80.
[18] Q. Wang, J. Liu, A Chang'e-4 mission concept and vision of future Chinese lunar exploration activities, Acta Astronaut. 127 (2016) 678–683.
[19] H. Liu, An overview of the space robotics progress in China, in: Proceedings of the International Symposium on Artificial Intelligence, Robotics and Automation in Space, I-SAIRAS 2014, European Space Agency, 2014, pp. 1–5.
[20] D. Sanz, M. Garzon, A. Barrientos, C. Rossi, A. Medina, A. Puiatti, Robotic deployment system for space exploration, in: Proc. of the 10th International Symposium on Artificial Intelligence, Robotics and Automation in Space, iSAIRAS, 2010.
[21] A. Trebi-Ollennu, W. Kim, K. Ali, O. Khan, C. Sorice, P. Bailey, J. Umland, R. Bonitz, C. Ciarleglio, J. Knight, N. Haddad, InSight Mars lander robotics instrument deployment system, Space Sci. Rev. 214 (2018) 1–18.
[22] EBAD, The EBAD TiNi™ frangibolt.
[23] D.B. Carte, N.K. Inamdar, M.P. Jones, R.A. Masterson, Design and test of a deployable radiation cover for the REgolith X-ray imaging spectrometer, in: 42nd Aerospace Mechanisms Symposium, NASA Goddard Space Flight Center, Washington, 2014.
[24] Santosh V. Vadawale, et al., Chandrayaan-3 APXS elemental abundance measurements at lunar high latitude, Nature 633, 327–331.
[25] S. Vijayan, et al., Chandrayaan-3 landing site evolution by South Pole Aitken basin and other impact craters, ICARUS 425, http://dx.doi.org/10.1016/j.icarus.2024.116329.